Current Chemistry Letters 14 (2025) 885–896

Contents lists available at GrowingScience

Current Chemistry Letters

homepage: www.GrowingScience.com

Exploring the optoelectronic and photovoltaic potential of Spiro-OMeTAD derivatives through quantum chemical investigations

Jaouad Ouhrir[a,b], Yahya Mekaoui[a], Ikram Mennas[b*], Souad Taj[a], Mohammed El idrissi[b*] and Bouzid Manaut[a]

[a]*Laboratory of Research in Physics & Engineering Sciences, Sultan Moulay Slimane University, Polydisciplinary Faculty, Beni Mellal, 23000, Morocco*
[b]*Team of Chemical Processes and Applied Materials, Sultan Moulay Slimane University, Polydisciplinary Faculty, Beni Mellal, 23000, Morocco*

C H R O N I C L E

Article history:
Received March 10, 2025
Received in revised form
June 2, 2025
Accepted July 7, 2025
Available online
July 7, 2025

Keywords:
TD-DFT
HTMs
ssDSCs
Optoelectronic properties
Charge Transport Properties

A B S T R A C T

This study provides an extensive evaluation of nine hole transport materials (HTMs) for solid-state dye-sensitized solar cells (ssDSCs), utilizing time-dependent density functional theory (TD-DFT) with the B3LYP level and the 6-31G(d,p) basis set. We investigated their electronic, optical and charge transport properties. The performance parameters of a photovoltaic cell, such as light harvesting efficiency (LHE), short-circuit current density (J_{SC}), and open-circuit voltage (V_{OC}), were analyzed. All the studied molecules exhibit energy band gaps ranging from 2.994 eV to 3.541 eV, confirming their ability to absorb light in the visible range. In addition to optical properties, the study explores charge transfer integrals, transport rates and mobility of charge, emphasizing the importance of efficient hole and electrons mobility and reduced charge recombination. These findings highlight the potential of these molecules as leading candidates for enhancing the efficiency of ssDSCs.

© 2025 by the authors; licensee Growing Science, Canada.

1. Introduction

The growing global population and the overexploitation of non-renewable energy sources have intensified the search for sustainable alternatives. Renewable energies, such as silicon-based photovoltaic technologies, have emerged as promising solutions. More recently, perovskite solar cells (PSCs) and dye-sensitized solid-state solar cells (ssDSCs), which incorporate hole-transporting materials (HTMs), have gained significant attention. In this context, organic dyes derived from bis-heterocyclic compounds are attracting increasing interest in the field of optoelectronics due to their finely tunable electronic properties. Their molecular structure provides remarkable flexibility, enabling precise adaptation to the specific requirements of devices such as photovoltaic cells. Recent studies have demonstrated their efficiency in light absorption and charge transport two critical factors for enhancing device performance[1–3]. Additionally, these dyes exhibit improved thermal and chemical stability, fulfilling the demands of sustainable technologies. Their conjugated structures and high functionalization potential facilitate the design of complex supramolecular architectures, leading to the development of more efficient and stable hole-transporting materials (HTMs). Furthermore, bis-heterocyclic compounds allow precise control over energy levels within active layers, making them indispensable components in the design of next-generation optoelectronic devices.

These types of molecules are important because they facilitate the movement of holes from the light-absorbing layers to the cathode. Spiro-OMeTAD 2,2',7,7-Tetrakis[N,N-di(4- methoxyphenyl)amino]-9,9-spirobifluorene) is the reference material for HTMs. This molecule has been extensively studied, regarding its properties, with S. Fantacci's Density

* Corresponding author
E-mail address ikrammennas321@gmail.com (I. Mennas) m.elidrissi2018@gmail.com (M. El Idrissi)

© 2025 by the authors; licensee Growing Science, Canada
doi: 10.5267/j.ccl.2025.7.001

Functional Theory (DFT) and Time-Dependent DFT (TD-DFT) calculations shedding light on its molecular, electronic, and optical properties across various oxidation states. These studies highlight why spiro-OMeTAD is considered a leading HTM in ssDSCs and organic light emitting devices (OLEDs)[4–12] Spiro-OMeTAD layer used in perovskite solar cells (PSCs) showed a certified power conversion efficiency of 25.34% with a record certified fill factor (FF) reaching 87.02%[13]. The design of HTMs focused on improving the charge transport parameters and neglecting the light absorption properties. All this leads us to ask a question what if HTMs could be designed to also contribute significantly to light absorption.

This research seeks to challenge the conventional boundaries of HTMs by exploring their potential to function not only as efficient charge transporters but also as light absorbers. This dual functionality could broaden the absorption spectrum, enhance photoconversion efficiency, and simplify the device architecture, leading to new strategies for improving solar cell performance. By reversing the traditional role of HTMs, we aim to determine whether they can be effectively utilized as dyes, thereby playing a more active role in the photoconversion process. To investigate this hypothesis, our study concentrated on five distinct families of HTMs, all derived from the widely recognized spiro-OMeTAD structure, as illustrated in Figure 1. The first family involves asymmetric modifications of the phenyl rings with additional alkyl chains attached to the spiro-OMeTAD core, leading to the development of compounds D92-D94[14]. The second family incorporates acridine units into a spirobifluorene-based molecular glass, resulting in compounds D95-D97[14]. Additionally, we synthesized compound D98 by introducing diphenylamine (DPA) units, and compound D99 by integrating xanthene within the spirobifluorene backbone. Finally, compound D100, also known as PST1, represents another novel derivative based on structural modifications of the spirobifluorene core[15]. In this study, we will explore not only the conventional charge transport capabilities of these HTMs but also their optical absorption characteristics. By systematically modifying the molecular framework of these spiro-OMeTAD derivatives, we aim to identify candidates capable of acting as dual-function materials serving as both HTMs and dyes. Such materials would have the potential to improve ssDSC performance by expanding the light absorption spectrum, facilitating more efficient hole transfer, and minimizing charge recombination losses. The findings of this study could open new avenues for innovative design approaches in organic and hybrid photovoltaics, potentially enabling the creation of more efficient, affordable, and simplified solar cell technologies.

2. Technical computation

In our study investigating the spatial configuration and electronic properties of various HTMs compounds, we used Gaussian 09 for the calculations[16]. We first constructed and optimized the molecular structures to their minimum energy conformations using molecular modeling software. To predict electronic transitions and optical properties, we applied time-dependent density functional theory (TD-DFT)[17,18], employing the B3LYP[19] functional known for its accuracy in electronic property prediction. We also used the 6-31G (p,d) basis set, which includes polarization functions to accurately describe the electronic structure. All the requested information regarding the reaction medium and the application technique has been added. Specifically, all calculations were performed in the gas phase without explicit solvent modeling, in order to highlight the intrinsic electronic properties of the dyes under investigation. This approach also allowed for a simplification of the computational treatment while ensuring methodological consistency across the different dye derivatives considered. **Fig. 2** shows the results of the optimization at the B3LYP/6-31G(d,p) base level of all dyes (D32-D100). The Cartesian XYZ coordinates of these optimized structures are shown in supplementary table S1-S9.

The evaluation of HTMs often prioritizes the value of the HOMO level due to its critical role in facilitating efficient hole transport. A deeper HOMO level in HTMs is associated with enhanced hole mobilities, as highlighted in prior studies [20]. To ensure the credibility and accuracy of our computational method, we used experimental HOMO values reported in the literature as reference points. As shown in **Table 1**, the differences between the HOMO values calculated using the B3LYP/6-31G(d,p) method and the corresponding experimental values were consistently within a reasonable range. This level of agreement, with deviations not exceeding 21.5%, validates the reliability of our computational approach and supports its applicability for predicting electronic properties of HTMs with reasonable accuracy.

Table 1. Comparison of calculated and experimental HOMO energy levels for all dyes.

	D92	D93	D94	D95	D96	D97	D98	D99	D100
$E_{HOMO}(eV)$	-4.107	-4.358	-4.299	-4.312	-4.331	-4.308	-4.173	-4.423	-4.293
$E_{HOMO}^{Exp}(eV)$	-4.95[21]	-5.08[21]	-5.02[21]	-4.92[22]	-4.92[22]	-4.93[22]	-5.07[23]	-5.12[24]	-5.15[15]
ΔE (eV)	0.843	0.722	0.721	0.608	0.589	0.622	0.897	0.697	0.857
$\frac{\Delta E}{E_{HOMO}}\%$	20.53	16.57	16.77	14.1	13.6	14.44	21.5	15.76	19.96

After the calculations, we analyzed parameters such as electronic energy levels, absorption spectra, and charge transport properties. Moreover, the FMOs, nonlinear optical properties, MEP, and electronic features of the stable structures were determined using the same approach. The optical absorption spectrum was produced with Gauss View 6.0[25], and its graph was rendered using gnuplot software[26].

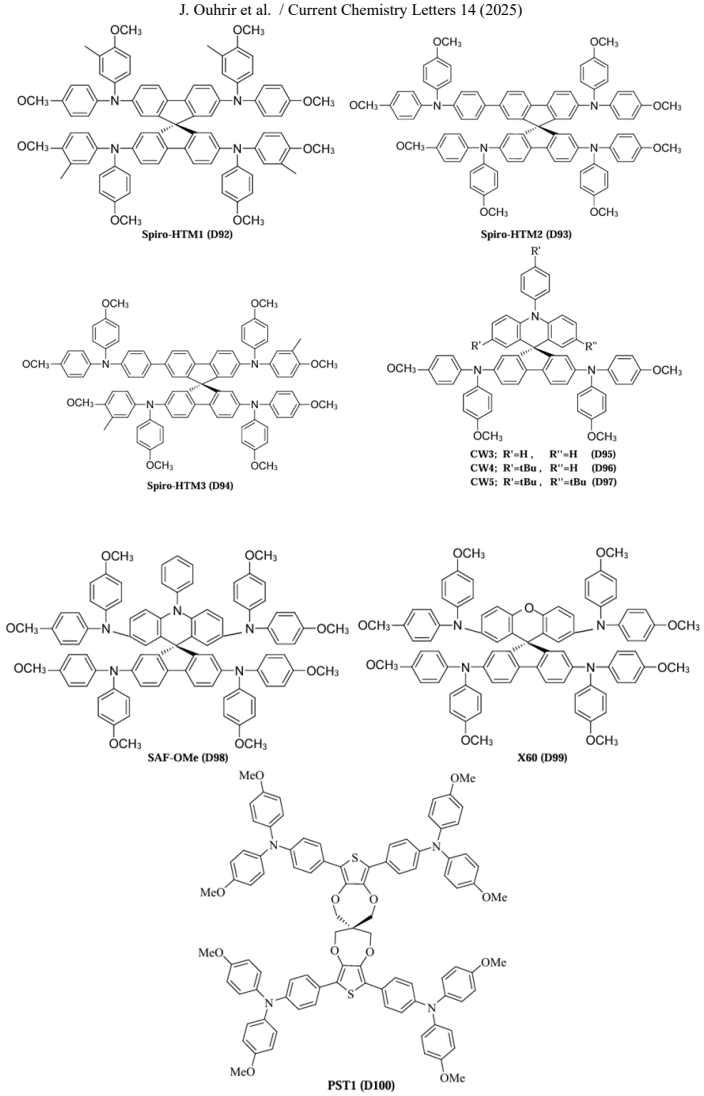

Fig. 1. Representation of the chemical structures of the studied dyes (D92–D100)

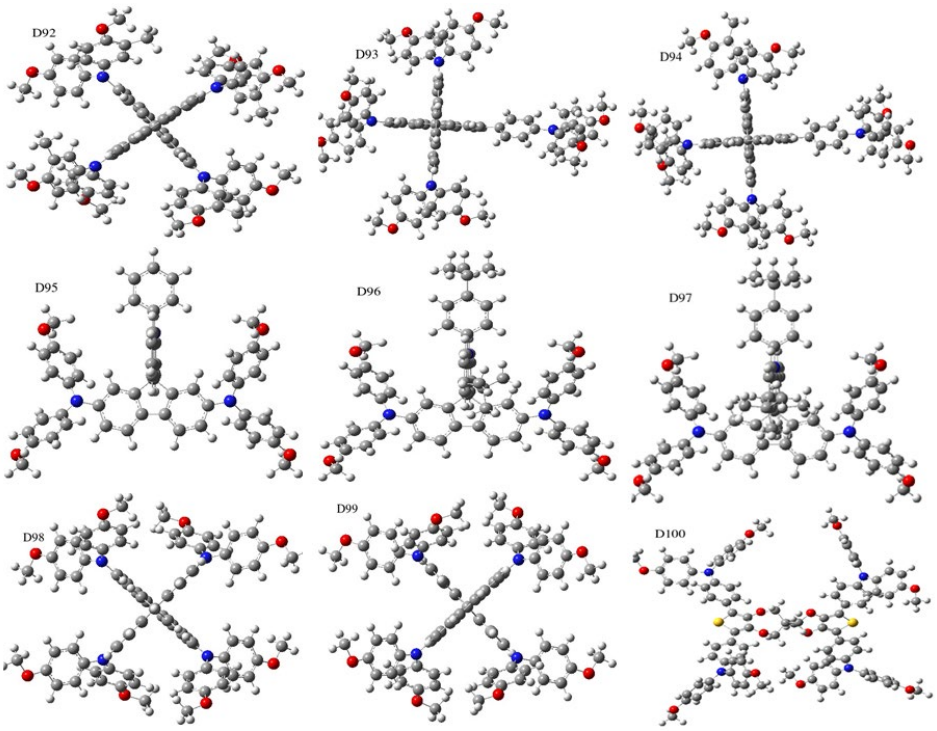

Fig. 2. The optimization results for all dyes (D92-D100) at the B3LYP/6-31G(d,p) basis level

3. Results and Analysis

3.1 Frontier molecular analysis

To investigate optoelectronic properties and assess charge transfer within molecules, we analyzed the HOMO and LUMO energy levels. Appropriate HOMO and LUMO energies significantly improve the hole transfer efficiency of HTMs. The FMOs provide insight into the charge density distributions across a molecule. **Fig. 3** depicts the HOMO and LUMO orbitals for the HTMs studied. Negative charges are indicated in red, while positive charges are shown in green. For most HTMs, the LUMO orbitals are centrally localized; however, in specific cases, such as D93, D94, and D95, they are situated on the terminal atoms.

Generally, the HOMO orbitals are mainly localized onto the central core. Additionally, in some samples, HOMO orbitals are more dispersed throughout the molecules. This suggests a more efficient interaction between the molecule's HOMO and the dye in the ssDSCs, leading to enhanced hole transport ability compared to electron transport.

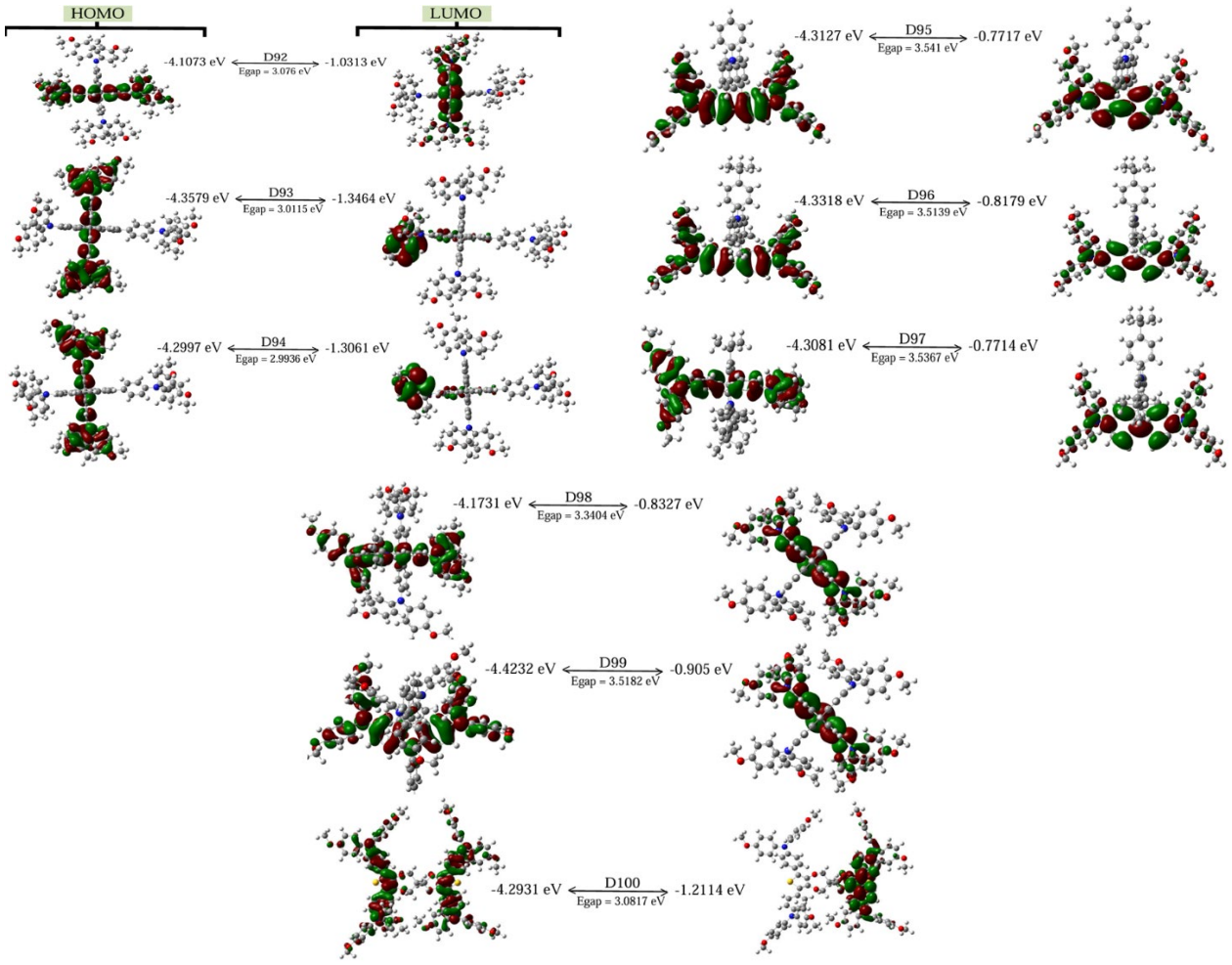

Fig. 3. HOMO/LUMO Energy and band gap analysis across all dyes

3.2 Electronic properties

The ionization potential (IP) and electron affinity (EA) can be deduced using these specific equations[27]

$$IP = -E_{HOMO},\ EA = -E_{LUMO} \tag{1}$$

Chemical reactivity descriptors are fundamental for studying the behavior and properties of molecules. Among the main global descriptors, we can find in particular chemical potential (μ), electronegativity (χ), electrophilicity (ω), hardness (η), and softness (S), can be computed using the following fundamental equations[27]:

$$\mu = \frac{1}{2}(EA + IP) \qquad \chi = \frac{1}{2}(EA + IP) \qquad \eta = \frac{1}{2}(EA + IP) \tag{2}$$

$$S = (2\eta)^{-1} \qquad \omega = \frac{\mu^2}{2\eta} \tag{3}$$

As shown in **Table 2**, D94 exhibits the lowest energetic gap (E_{gap} = 2.994 eV), rendering it the softest (S = 0.334 eV) molecule among the compounds analyzed. Conversely, D95 present the highest energy gap (E_{gap} = 3.541 eV). D92 has the highest HOMO energy (E_{HOMO} = −4.107 eV), making it the most effective electron donor. Additionally, dye 98, with the lowest LUMO energy (E_{LUMO} = −0.833 eV), is identified as the optimal electron acceptor.

Table 2. The LUMO and HOMO energy levels, energy gap, and global reactivity parameters of the studied dyes calculated using TD-DFT/B3LYP/6-31G(d,p)

Dyes	D92	D93	D94	D95	D96	D97	D98	D99	D100	TiO_2[28]
E_{HOMO}(eV)	-4.107	-4.358	-4.299	-4.312	-4.331	-4.308	-4.173	-4.423	-4.293	-7.16
E_{LUMO}(eV)	-1.031	-1.346	-1.306	-0.772	-0.818	-0.771	-0.833	-0.905	-1.211	-4.00
Egap(eV)	3.076	3.012	2.994	3.541	3.514	3.537	3.340	3.518	3.082	3.16
IP(eV)	4.107	4.358	4.299	4.313	4.332	4.308	4.173	4.423	4.293	7.16
EA(eV)	1.031	1.346	1.306	0.772	0.818	0.772	0.833	0.905	1.211	4.00
μ (eV)	-2.569	-2.852	-2.803	-2.542	-2.575	-2.540	-2.503	-2.664	-2.752	-5.58
χ (eV)	2.569	2.852	2.803	2.542	2.575	2.540	2.503	2.664	2.752	5.58
η (eV)	1.538	1.506	1.497	1.771	1.757	1.768	1.670	1.759	1.541	1.580
S (eV)	0.325	0.332	0.334	0.282	0.285	0.283	0.299	0.284	0.324	0.316
ω (ev)	2.146	2.701	2.623	1.825	1.887	1.824	1.875	2.017	2.458	9.853

Based on **Table 2**, the energy gap decreases in the following order: D95 > D97 > D99 > D96 > D98 > TiO_2 > D100 > D92 > D93 > D94. As indicated in **Table 2**, the electronegativity of all the compounds is lower than that of TiO_2, signifying that TiO_2 exhibits a stronger electron-attracting capability. On the other hand, the dyes are effective in releasing electrons. Moreover, the chemical potentials of these dyes exceed that of TiO_2, reflecting their enhanced capacity to transfer electrons to the semiconductor. This underscores their suitability as promising electron donors for solar cell applications [29].

3.2 Molecular electrostatic charge potential

The molecular electrostatic potential (MEP), closely related to electron density, is an essential descriptor for identifying sites of electrophilic and nucleophilic attack as well as hydrogen bond interactions[30,31].

In this study, the MEP was evaluated using the TD-DFT/B3LYP/6-31G (d,p) method, as shown in **Fig. 4**. This figure uses a color-coded diagram to illustrate electrostatic potential values, with the most negative regions in red, indicating likely sites for electrophilic attacks, and the most positive regions in dark blue, highlighting preferred sites for nucleophilic attacks. Notably, the most negative potential is concentrated around the nitrogen and oxygen atoms, suggesting these areas are prone to electrophilic attacks, while green represents neutral regions[32].

Through our observation of the electrostatic maps, we see that oxygen is covered in red in all the dyes, indicating these areas are rich in electrons. The electrostatic surface potential (ESP) maps of all dyes, calculated and presented in **Fig. 4**, reveal significant differences in charge dispersion. The dominant color in dyes 93 and 100 is cyan, indicating a positive potential, which suggests these dyes are prime candidates to be electron acceptors. Conversely, the rest of the dyes are dominated by colors close to yellow and red, indicating a negative potential, making them candidates as electron donors.

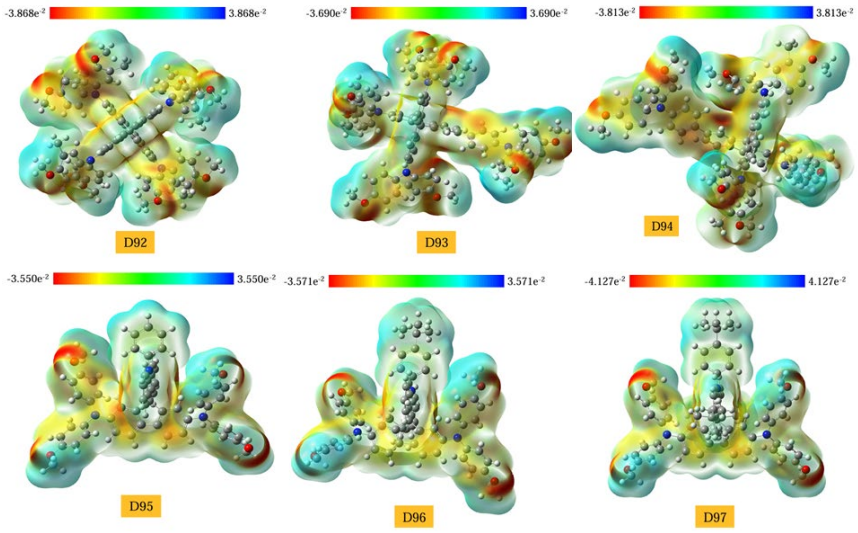

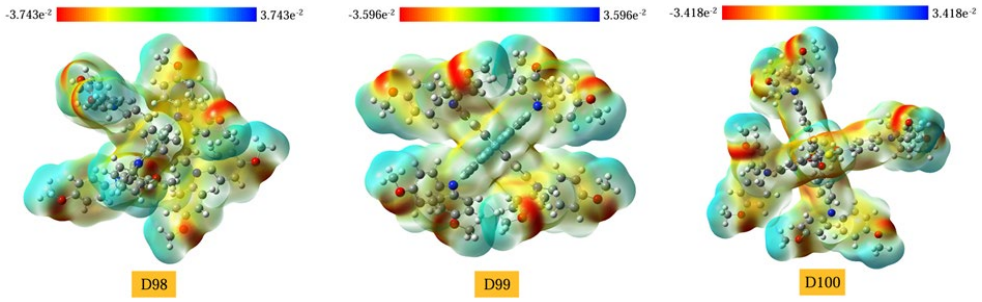

Fig. 4. ESP maps of all dyes

3.4 Density of states

Density of states (DOS) reveals how electrons are distributed across different energy levels. **Fig. 5** presents the DOS for all the dyes, where peaks indicate energy levels with available states, and zero DOS means no available positions at that energy level. The green part corresponds to the occupied orbitals, while the red part represents the virtual (or unoccupied) orbitals of the ground State. These vacant orbitals can only be occupied when electrons are excited[33]. The presence of two prominent peaks in the DOS in the virtual orbital region confirms the probability of light absorption. The virtual orbitals represent possible excited states of the molecule, and DOS peaks indicate the availability of these states at specific energies.

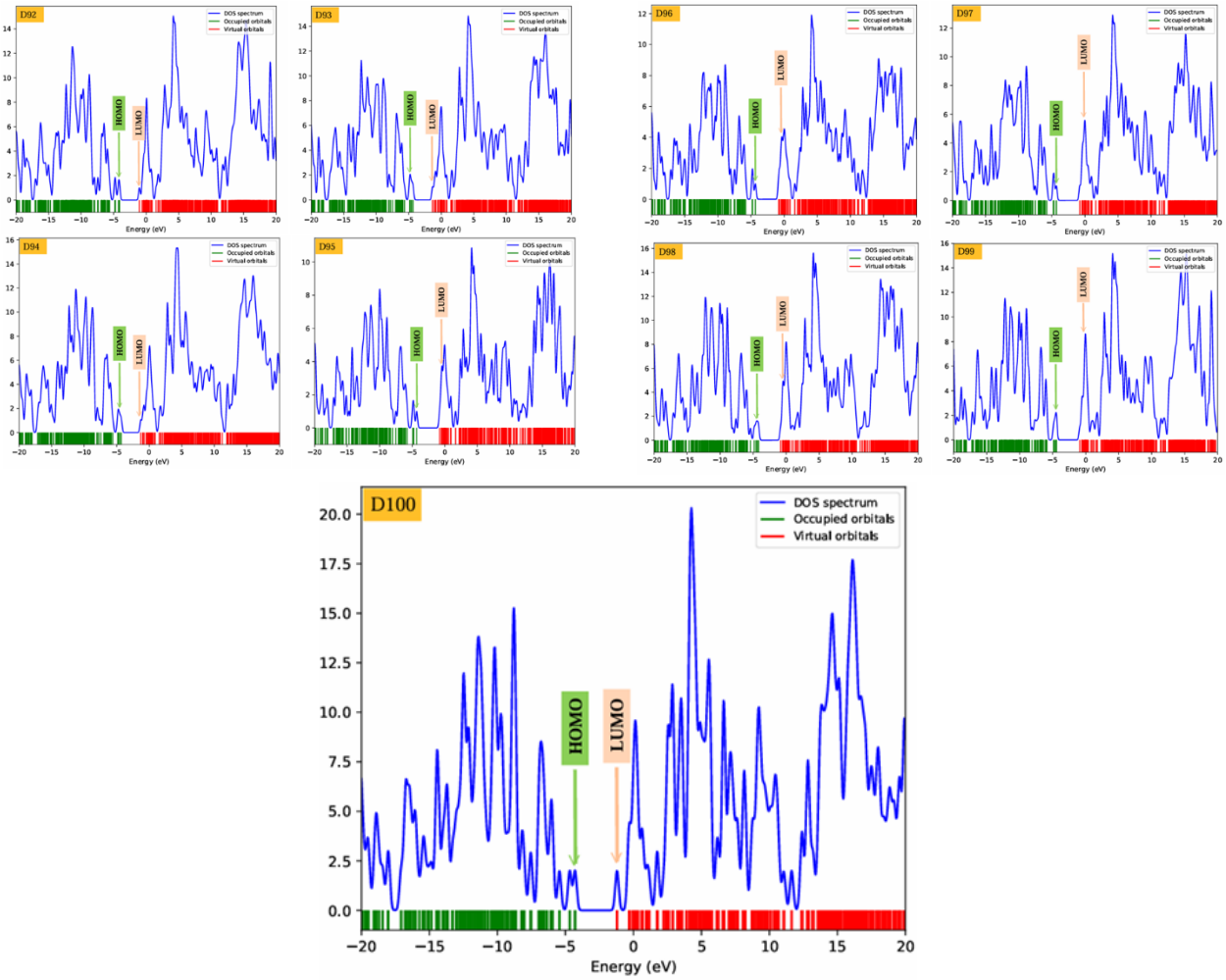

Fig. 5. The density of state plots of all dyes

4. Absorption properties

The maximum absorption wavelengths (λ_{max}), oscillator strength (f), and excitation energy (E_{ex}) for all compounds are presented in **Table 3**. The high oscillator strength values signify that these transitions are predominant. The order of λ_{max} values is found to be D94 > D100 > D93 > D96 > D99 > D98> D92> D97> D95, indicating that D94 absorbs at the

longest wavelength while D95 absorbs at the shortest. Additionally, the order of the excitation energies E_{ex} values is D95 > D97 >D92 > D98 > D99 > D96 > D93 > D100 > D94, indicating that D95 has the highest excitation energy while D94 has the lowest. The transitions from the HOMO to the LUMO are the most feasible, indicating the primary excitation process in these dye molecules.

Table 3. The absorption characteristics of the examined dyes (D92 to D100)

Dyes	Transition (%)				λ_{max} (nm)	f(Hz)	E_{ex} (eV)
D92	H-1	⟶	L	(98%)	440.38	0.9086	2.8154
	H	⟶	**L+1**	**(94%)**	**403.29**	**0.9528**	**3.0743**
D93	H	⟶	L	(84%)	458.61	0.0298	2.7035
	H-1	⟶	**L**	**(79%)**	**452.96**	**0.1108**	**2.7372**
	H	⟶	L+1	(91%)	438.74	0.0520	2.8259
D94	H	⟶	L	(88%)	461.42	0.0237	2.6870
	H-1	⟶	**L**	**(83%)**	**455.41**	**0.1143**	**2.7225**
	H	⟶	L+1	(91%)	441.13	0.0490	2.8106
D95	**H**	⟶	**L**	**(98%)**	**401.75**	**1.0157**	**3.0861**
	H	⟶	L+3	(93%)	373.99	0.0212	3.3152
	H	⟶	L+2	(47%)	363.38	0.0008	3.4120
D96	**H**	⟶	**L**	**(98%)**	**405.88**	**0.9363**	**3.0547**
	H	⟶	L+1	(97%)	390.91	0.0053	3.1717
	H	⟶	L+2	(87%)	373.85	0.0214	3.3164
D97	**H**	⟶	**L**	**(98%)**	**403.08**	**0.9419**	**3.0759**
	H	⟶	L+1	(93%)	373.15	0.0216	3.3226
	H-1	⟶	L	(98%)	369.15	0.0000	3.3586
D98	H	⟶	L	(99%)	432.57	0.0001	2.8662
	H	⟶	L+2	(96%)	405.27	0.0001	3.0593
	H-1	⟶	**L**	**(97%)**	**403.62**	**0.8216**	**3.0718**
D99	**H**	⟶	**L**	**(98%)**	**405.83**	**0.8529**	**3.0551**
	H	⟶	L+2	(70%)	376.49	0.0126	3.2932
D100	H	⟶	L	(51%)	455.41	1.4387	2.7225
	H	⟶	**L+1**	**(55%)**	**454.52**	**1.4390**	**2.7278**
	H-1	⟶	L	(52%)	436.35	0.0023	2.8414

Fig. 6 illustrates the absorption spectra of various dyes, showing distinct maximum absorption peaks at specific wavelengths. Dye D100 exhibits the highest absorption peak with a maximum value of 1.17×10^5 at 454 nm, indicating strong absorption in the blue wavelength range of the spectrum and suggesting significant potential for efficient light harvesting and charge generation. Dye D92 follows with a substantial peak value of 6.81×10^4 at 420 nm, also in the blue region, demonstrating a robust capability for light absorption. For Dyes D95, D97, D96, D99 and D98 which exhibit moderate peaks absorption values of 4.17×10^4, 3.87×10^4, 3.86×10^4, 3.49×10^4 and 3.32×10^4 at 401 nm, 402 nm, 404 nm, 406 nm and 403 nm respectively, the absorption occurs in the violet range of the visible spectrum, it's very close to the ultraviolet (UV). Lastly, for Dye D93 and D94 exhibits a small peak with a maximum value of 7.71×10^3 and 7.49×10^3 at 450 nm and 452 nm respectively, the absorption places these dyes in the visible region, specifically in the blue portion of the spectrum.

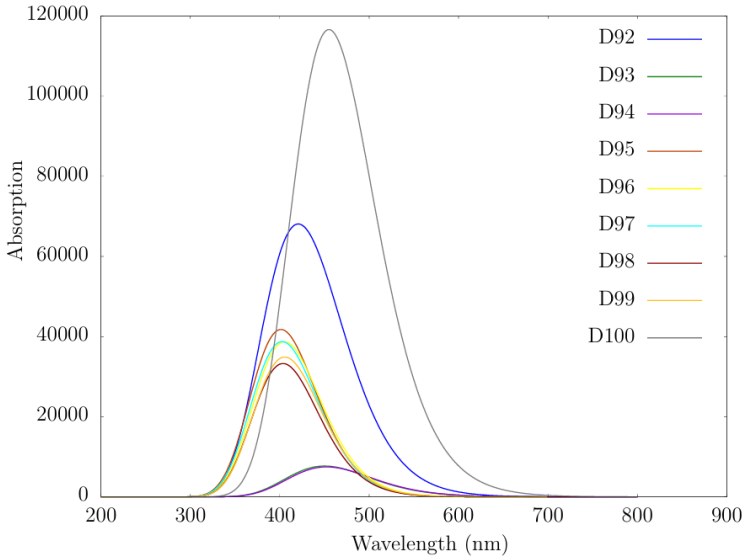

Fig. 6. Absorption spectra of all dyes as a function of wavelength, highlighting the maximum absorption peaks and their corresponding intensities

5. Photovoltaic properties

The ssDSC convert light energy into electricity through a process inspired by photosynthesis. When a photon strikes the cell, it excites an electron in the dye adsorbed on the titanium dioxide layer. This excited electron is then injected into the semiconductor. To maintain electrical neutrality, ions move through HTMs, which regenerate the oxidized dye and complete the electrical circuit. These processes generate a direct electric current, in addition to these electrons, the HTMs can produce extra electrons that will be injected into the conduction band of TiO_2, in this part we will try to calculate the parameters which affect this additional current, effectively converting solar energy into usable electricity. The efficiency of this conversion is determined by the following equation[34]:

$$\eta = \frac{J_{SC} V_{OC} FF}{P_{Solar}} \tag{4}$$

where P_{Solar} indicates the incident power density, J_{SC} is the symbol of the current density at short-circuit, while V_{OC} stands for the voltage at open-circuit, and FF refers to the fill factor. Hence, both J_{SC} and V_{OC} are essential aspects in determining the effectiveness of Grätzel cells (DSSCs).

The density of the short-circuit current (J_{SC}) can be evaluated using Eq. (5) [35]:

$$J_{SC} = \int LHE(\lambda) \Phi_{inj} \xi_{collect} d\lambda \tag{5}$$

The light harvesting efficiency is denoted by LHE(λ). To have a maximum photocurrent, the LHE must be high, which can be expressed as[36-37].

$$LHE = 1 - 10^{-f} \tag{6}$$

In the formula, the symbol of denotes the oscillator strength of the sensitizer related to the wavelength λ_{max}. Higher oscillator strength indicates a stronger oscillation and therefore better light harvesting. The highest LHE was observed for dye D100, with a value of 0.9636, indicating superior light absorption capabilities. This is consistent with its high oscillator strength (f = 1.439), which implies strong electronic transitions and efficient photon capture. Consequently, D100 stands out as the most promising candidate for maximizing light absorption in the visible spectrum, a crucial factor for achieving high photocurrent densities in DSSCs. Dyes D95, D96, and D97 also exhibited robust LHE values, ranging from 0.8842 to 0.9036, suggesting that they are capable of harvesting a substantial portion of incident light. These dyes show strong absorption in the violet region of the spectrum. On the other hand, dyes D93 and D94 demonstrated a lower LHE values of 0.2252 and 0.2314, respectively. These values reflect a relatively weak interaction with incident light, which can be attributed to their lower oscillator strengths (f = 0.1108 and 0.1143). As a result, their capacity to generate a high photocurrent is limited. However, even with high light harvesting, a significant injection yield (Φ_{inject}) according to Eq. (5) could lead to large short-circuit current (J_{SC}) values. The injection yield (Φ_{inject}) is connected to the injection driving force (ΔG_{inject}) by[38]

$$\Delta G_{inject} = E^{dye*} - E_{CB} \tag{7}$$

in which E^{dye*} is the energy of the excited dye's oxidation potential and the TiO_2 conduction band's reduction potential is identified as E_{CB} (E_{CB} = -4 eV), E^{dye*} could be obtained by[39]

$$E^{dye*} = E^{dye} - E_{00} \tag{8}$$

where E^{dye} is the dye's ground-state oxidation potential energy and E_{00} is the electronic vertical transition energy correlating to the wavelength λ_{max}[40]. **Table 4** indicates that the ΔG_{inject} values for the pigments are negative. This implies that the conduction band of TiO_2 lies below the excited state of the dyes, promoting the injection of electrons into the TiO_2 conduction band without requiring external energy.

The open circuit photovoltage V_{OC} in DSSCs can be computed using the formula[41]

$$eV_{OC} = E_{LUMO} - E_{CB} \tag{9}$$

where E_{LUMO} denotes the LUMO energy level of the organic dye, and E_{CB} represents the conduction band of the semiconductor (with TiO_2 = -4.0 eV). From **Table 4**, we observe that the V_{OC} values are quite high, on the order of 3 eV. At first glance, this seems beneficial for increasing the efficiency of the cells. However, referring to the V_{OC} formula which represents the difference between the LUMO energy of the dye and the conduction band energy level of TiO_2 this difference should ideally be between 0.6 V and 0.8 V[42]. That is, the LUMO and the conduction band must be close enough

to ensure that the electron moves efficiently in one direction. For our study to be effective, we must select a suitable semiconductor.

Table 4. Ground-state oxidation potential (E^{dye}), excited-state oxidation potential (E^{dye*}), electron injection free energy (ΔG_{inject}), total regeneration energy (ΔG_{reg}), and open-circuit voltage (V_{OC}) values for all dyes

Dyes	D92	D93	D94	D95	D96	D97	D98	D99	D100
f	0.9528	0.1108	0.1143	1.0157	0.9363	0.9419	0.8216	0.8529	1.439
LHE	0.8885	0.2252	0.2314	0.9036	0.8842	0.8857	0.849	0.8597	0.9636
E^{dye*}**(eV)**	1.033	1.621	1.577	1.227	1.277	1.232	1.101	1.368	1.565
ΔG**inject(eV)**	-2.967	-2.379	-2.423	-2.773	-2.723	-2.768	-2.899	-2.632	-2.435
eV$_{OC}$ (eV)	2.969	2.654	2.694	3.229	3.182	3.229	3.167	3.095	2.789

6. Charge Transfer Integrals and Electron/Hole Transport Rates

An additional measure used to assess the charge transport in molecules is the charge transfer integral (t). This parameter is associated with the FMOs in the dimer arrangement. Using Koopman's theorem, the charge transfer integral can be calculated using the following equation[16,43]:

$$t_{electron} = \frac{1}{2}\left(E_{LUMO+1} - E_{LUMO}\right) \tag{10}$$

$$t_{hole} = \frac{1}{2}\left(E_{HOMO} - E_{HOMO-1}\right) \tag{11}$$

The reorganization energy is divided into two parts: internal (λ_{int}) and external (λ_{ext}). Internal reorganization energy refers to structural changes in the molecule due to polarization, while external reorganization energy reflects the influence of the surrounding environment. Given that the external environment has minimal impact on electron mobility, the contribution of λ_{ext} is considered negligible, and this study focuses on λ_{int} only[44]. As a result, the hole reorganization energy (λ_h) and electron reorganization energy (λ_e) are calculated using the following equation[44]:

$$\lambda_{electron} = \left[E_0^{anion} - E_{anion}\right] + \left[E_{anion}^0 - E_0\right], \tag{12}$$

$$\lambda_{hole} = \left[E_0^{cation} - E_{cation}\right] + \left[E_{cation}^0 - E_0\right]. \tag{13}$$

In these equations, E_0^{cation} and E_0^{anion} represent the energies of the cation and anion, respectively, calculated from the optimized neutral molecule. E_{anion} and E_{cation} are the energies of the cation and anion derived from the optimized cation and anion geometries. E_0 is the energy of the neutral molecule in its ground state, while E_0^{cation} and E_0^{anion} correspond to the energies of the neutral molecule obtained from the relaxed cation and anion geometries.

The expression for k_{CT} in the absence of a barrier can be written as follows[45]:

$$\lambda_{CT}^{hole/electron} = \sqrt{\frac{\pi}{\lambda^{hole/electron} K_B T}} \frac{t_{hole/electron}^2}{h} e^{\left(\frac{\lambda^{hole/electron}}{4K_B T}\right)} \tag{14}$$

In this equation, k_B represents the Boltzmann constant, t is the charge transfer, T is the temperature in absolute terms (298 K), and is the reduced Planck's constant. The charge transfer rate, k_{CT}, is primarily influenced by the charge transfer integral and the reorganization energy. The carrier mobility is an important parameter for evaluating the efficiency of hole or electron transport in a molecule, and it can be calculated using Einstein's equation[46,47]:

$$\mu_{mob} = \frac{eD}{K_B T} \tag{15}$$

Here, e denotes the electron charge and D represents the diffusion coefficient. For one-dimensional, D can be calculated using the following equation[47-49]:

$$D = \frac{t^2}{2} k_{CT}^{hole/electron} \tag{16}$$

where l indicates the distance between the two interacting molecules. Charge transfer integrals (CTIs) are crucial for understanding the speed at which electrons are transferred from an excited donor molecule to an excited acceptor molecule.

In our study, we have explored nine specific molecules, and the results, as summarized in **Table 5**, reveal distinct trends for electron and hole CTIs.

Table 5. Calculated charge transport rates and charge transfer integrals for all dyes at the TD-DFT B3LYP/6-31G(d,p) computational method

Dyes	$\lambda_{electron}$ (eV)	λ_{hole} (eV)	$t_{electron}$ (eV)	t_{hole} (eV)	$k_{CT}^{electron}$ (s^{-1})	k_{CT}^{hole} (s^{-1})	$\mu_{mob}^{electron}$ (cm^2/Vs)	μ_{mob}^{hole} (cm^2/Vs)
D92	0.7123	0.3355	0.2161	0.0758	1.60×10^{12}	1.13×10^{13}	1.62×10^{-3}	1.14×10^{-2}
D93	0.6894	0.4113	0.1512	0.1096	9.97×10^{11}	1.02×10^{13}	1.68×10^{-3}	1.71×10^{-2}
D94	0.9332	0.5321	0.1512	0.1138	7.98×10^{10}	2.97×10^{12}	2.13×10^{-4}	7.92×10^{-3}
D95	0.8876	0.2871	0.1285	0.2280	9.22×10^{10}	1.76×10^{14}	1.90×10^{-4}	3.64×10^{-1}
D96	0.7712	0.3511	0.0558	0.2155	5.78×10^{10}	7.65×10^{13}	8.52×10^{-5}	1.13×10^{-1}
D97	0.8002	0.2112	0.1690	0.1830	3.93×10^{11}	2.78×10^{14}	6.91×10^{-4}	4.88×10^{-1}
D98	0.7818	0.1358	0.1381	0.0990	3.18×10^{11}	2.11×10^{14}	4.90×10^{-4}	3.25×10^{-1}
D99	0.9567	0.3127	0.1563	0.0247	6.71×10^{10}	1.54×10^{12}	1.52×10^{-4}	3.50×10^{-3}
D100	0.8933	0.4787	0.0037	0.0059	7.02×10^{07}	1.42×10^{10}	2.00×10^{-7}	4.04×10^{-5}

The sequence of electron charge transfer integrals among the molecules is as follows, increasing progressively: D100 < D96 < D95 < D98 < D93 < D94 < D99 < D97 < D92. Conversely, the hole CTIs demonstrate a decreasing order: D95 > D96 > D97 >D94 > D93 > D98 > D92 > D99 > D100. These results highlight that the electron CTI values range between 0.0037 and 0.2161 eV, whereas the hole CTIs range from 0.0059 to 0.2280 eV. Notably, the molecule D92 exhibits superior charge separation and extraction efficiency at the interface of the photoactive layer and electron acceptor. This efficiency is reflected in D92's highest electron CTI and lowest hole CTI. **Table** 5 further indicates that for molecules D92 to D100, the hole transport coefficient (k_{CT}^{hole}) surpasses the electron transport coefficient ($k_{CT}^{electron}$). Consequently, these molecules could be categorized as effective organic electron transport materials. The hole mobility (μ_{mob}^{hole}) among the modeled molecules ranges from 4.04×10^{-5} to 0.488 cm^2/Vs, with D97 showcasing the highest value and D100 the lowest. In contrast, electron mobilities ($\mu_{mob}^{electron}$) are generally lower compared to their corresponding hole mobilities, varying from 2.00×10^{-7} to $1.68\times10^{-3}cm^2$/Vs, with D93 having the highest and D100 the lowest values.

7. Conclusion

Utilizing TD-DFT with the B3LYP functional and the 6-31G(d,p) basis set, we conducted a detailed analysis of various HTMs. The optical properties demonstrate that dye D100 has the highest absorption peak, with a maximum value of 1.17 × 10^5 at 454 nm. Strong absorption of light capacity was also demonstrated using dye D92, which had a prominent peak at 420 nm. Dyes D95, D97, and D98, on the other hand, showed more modest absorption, mostly across the violet to near-ultraviolet spectrum. According to the photovoltaic characteristics, dye D100 has the maximum light harvesting efficiency (LHE). The V_{OC} values are quite high, on the order of 3 eV. The negative values of ΔG_{inject} imply that the TiO_2 conduction band lies below the excited state of the dyes, favoring electron injection into the TiO_2 conduction band. Concerning charge transport characteristics, D100 demonstrates limited mobility for both electrons and holes. Conversely, the electron in D93 and the hole in D97 exhibit greater mobility. Despite D100's significant capacity for light absorption and the generation of hole-electron charge pairs, the mobility of these charges is inferior to that of other dyes. Finally, we conclude that HTMs, as dyes, present an additional avenue for exploration in future studies.

References

1. Al-Jumaili M.H.A., Hamad A.A. , E. Hashem H., Hussein A.D., Muhaidi M.J., Ahmed M.A., A. Albanaa H.A. , Siddique F., Bakr E.A. **(2023)** Comprehensive review on the Bis–heterocyclic compounds and their anticancer efficacy. *J. Mol. Struct*., 1271, 133970. https://doi.org/10.1016/j.molstruc.2022.133970
2. Iftikhar R., Khan F.Z., Naeem N. (2024) Recent synthetic strategies of small heterocyclic organic molecules with optoelectronic applications: a review. *Mol Divers*., 28, 271–307. https://doi.org/10.1007/s11030-022-10597-0
3. Kula K., Jasiński R. **(2024)** Synthesis of bis(het)aryl systems via domino reaction involving (2E,4E)-2,5-dinitrohexa-2,4-diene: DFT mechanistic considerations. *Chem Heterocycl Comp*., 60,600–610. https://doi.org/10.1007/s10593-025-03383-x
4. Yang X., Luo X., Guo Y. **(2024)** Recent advances in cross-linkable organic hole-transporting materials for perovskite optoelectronics. *J. Mater. Chem. C.*, 12(47), 18952–18971. https://doi.org/10.1039/D4TC04111A
5. Kerraj S., Arif A., Aboulouard A., Salah M., El idrissi M., Belaaouad S. **(2025)** Exploring the optoelectronic and

photovoltaic properties of Ru-arene complexes: DFT and TD-DFT insights into DSSC performance. *J. Organomet. Chem.*, 1034, 123650. https://doi.org/10.1016/j.jorganchem.2025.123650.

6. Arif A., Aboulouard A., Can M., Bensemlali M., Boulghalat M., El idrissi M. **(2023)** Computational study of the optical and photovoltaic properties of novel dyes for dye-sensitized solar cell applications. *Matériaux & Techniques.*, 111, 5–6. https://doi.org/10.1051/mattech/2023036
7. Bai Y., He J., Ran R., Zhou W., Wang W., Shao Z. **(2024)** Complex metal oxides as emerging inorganic hole-transporting materials for perovskite solar cells. *Small.*, 20(25), 2310227. https://doi.org/10.1002/smll.202310227.
8. Singh BP., Goyal SK., Kumar P. **(2021)** Solar PV cell materials and technologies: analyzing the recent developments. *Mater. Today. Proc.*, 43(5), 2843–2849. https://doi.org/10.1016/j.matpr.2021.01.003.
9. Sikiru S., Oladosu TL., Amosa TI. **(2022)** Recent advances and impact of phase change materials on solar energy: a comprehensive review. *J. Energy Storage.*, 53, 105200. https://doi.org/10.1016/j.est.2022.105200
10. O'Regan B., Grätzel M. **(1991)** A low-cost, high-efficiency solar cell based on dye-sensitized colloidal TiO_2 films. *Nature.*, 353, 737–740. https://doi.org/10.1038/353737a0
11. Hua Y., Zhang J., Xu B **(2016)** Facile synthesis of fluorene-based hole transport materials for highly efficient perovskite solar cells and solid-state dye-sensitized solar cells. *Nano Energy.*, 26, 108–113. https://doi.org/10.1016/j.nanoen.2016.05.006.
12. Fantacci S., De Angelis F., Nazeeruddin MK., Grätzel M. **(2011)** Electronic and optical properties of the Spiro-MeOTAD hole conductor in its neutral and oxidized forms: a DFT/TDDFT investigation. *J. Phys. Chem. C.*, 115(46), 23126–23133. https://doi.org/10.1021/jp207968b.
13. Gao S., Li X., Cao R. **(2024)** Hot pure oxygen accelerated oxidation of Spiro-OMeTAD for efficient perovskite solar cells with a record certified fill factor exceeding 87%. *ACS Energy Lett.*, 9(10), 5037–5044. https://doi.org/10.1021/acsenergylett.4c01912.
14. Agarwala P., Kabra D. **(2017)** A review on triphenylamine (TPA)-based organic hole transport materials for dye-sensitized solar cells and perovskite solar cells: evolution and molecular engineering. *J. Mater. Chem. A.*, 5, 1348–1373. https://doi.org/10.1039/C6TA08449D.
15. Ganesan P., Fu K., Gao P. **(2015)** A simple spiro-type hole transporting material for efficient perovskite solar cells. *Energy Environ. Sci.*, 8, 1986–1991. https://doi.org/10.1039/C4EE03773A.
16. Aboulouard A., Demir N., Can M., El idrissi M. **(2023)** Electronic .and optical aspects of novel quinoxaline derivatives as electron donor materials for bulk heterojunction solar cells. *J. Mol. Graph. Model.*, 121, 108462. https://doi.org/10.1016/j.jmgm.2023.108462.
17. Guerra CF., Snijders JG., te Velde G., Baerends EJ. **(1998)** Towards an order-N DFT method. *Theor. Chem. Acc.*, 99, 391–403. https://doi.org/10.1007/s002140050353.
18. Laurent AD., Jacquemin D. **(2013)** TD-DFT benchmarks: a review. *Int. J. Quantum Chem.*, 113(17), 2019–2039. https://doi.org/10.1002/qua.24438.
19. Civalleri B., Zicovich-Wilson CM., Valenzano L., Ugliengo P. **(2008)** B3LYP augmented with an empirical dispersion term (B3LYP-D*) as applied to molecular crystals. *CrystEngComm.*, 10(4), 405–410. https://doi.org/10.1039/B715018K.
20. Sun ZZ., Xu YL., Zhu R., Liu HY. **(2018)** How to stabilize the HOMO levels and improve the charge transport properties of hole-transporting materials? Probing the effects of molecular symmetry. *Org. Electron.*, 63, 86–92. https://doi.org/10.1016/j.orgel.2018.09.013.
21. Malinauskas T., Luksiene DT., Sens R. **(2015)** Enhancing thermal stability and lifetime of solid-state dye-sensitized solar cells via molecular engineering of the hole-transporting material Spiro-OMeTAD. *ACS Appl. Mater. Interfaces.*, 7(21), 11107–11116. https://doi.org/10.1021/am5090385.
22. Li MH., Hsu CW., Shen PS. **(2015)** Novel spiro-based hole transporting materials for efficient perovskite solar cells. *Chem. Commun.*, 51, 15518–15521. https://doi.org/10.1039/C5CC04405G.
23. Wang YK., Yuan ZC., Shi GZ. **(2016)** Dopant-free spiro-triphenylamine/fluorene as hole-transporting material for perovskite solar cells with enhanced efficiency and stability. *Adv. Funct. Mater.*, 26, 1375–1381. https://doi.org/10.1002/adfm.201504245.
24. Mohammadnezhad M., Mohammadi H., Sabzyan H., Rahmani Z., Elmi F. **(2017)** Computational study of new triphenylamine derivatives as hole-transporting materials in perovskite solar cells. *J. Comput. Electron.*, 16(4), 1142–1150. https://doi.org/10.1007/s10825-017-1097-8.
25. Wang T., Xie Y., Dou Y. **(2018)** Theoretical design and investigation of carbazole-based hole transport materials for perovskite solar cells. *Synth. Met.*, 235, 9–18. https://doi.org/10.1016/j.synthmet.2017.11.013.
26. Joshi P., Deshmukh M., Rawal SK., Sakle SS., Kapse V. **(2023)** Molecular engineering of TPA derivatives for dye-sensitized solar cells: a DFT and TD-DFT study. *Opt. Mater.*, 139, 113710. https://doi.org/10.1016/j.optmat.2023.113710.
27. Yoon HM., Lee SY., Choi H. **(2018)** Novel carbazole-based hole transport materials for perovskite solar cells with high efficiency and long-term stability. *Adv. Funct. Mater.*, 28(20), 1801204. https://doi.org/10.1002/adfm.201801204.
28. Malinauskas T., Tomkute-Luksiene D., Sens R. **(2014)** New materials for organic and hybrid solar cells: towards dopant-free hole transporting layers. *Chem. Soc. Rev.*, 43, 622–659. https://doi.org/10.1039/C3CS60232C.
29. Sun ZZ., Xu YL., Zhu R., Liu HY. **(2018)** Probing the effects of molecular symmetry on the HOMO levels and charge transport properties of hole-transporting materials. *Org. Electron.*, 63, 86–92. https://doi.org/10.1016/j.orgel.2018.09.013.

30. Bai Y., Yu H, Ma Z. **(2018)** A solution-processable spiro-type hole transport material for perovskite solar cells with high efficiency and long-term stability. *ACS Appl. Energy Mater.*, 1(1), 114–121. https://doi.org/10.1021/acsaem.7b00013
31. Kerraj S., Arif A., Boulghalat M., El idrissi M. **(2024)**. Unveiling the impact of donor moieties on the optoelectronic and charge transport properties of new hole transporting materials: DFT insights. *ACS Appl. Energy Mater.*, 125, 108789. https://doi.org/10.1016/j.jmgm.2024.108789.
32. Nikzad-Langerodi R., Sarvari N., Razi N., Behjati S. (2017) Theoretical design of spiro-based hole transporting materials for perovskite solar cells. *Org. Electron.*, 50, 191–199. https://doi.org/10.1016/j.orgel.2017.07.035.
33. Gao P., Grätzel M., Nazeeruddin MK. **(2014)** Organohalide lead perovskites for photovoltaic applications. *Energy Environ. Sci.,7*, 2448–2463. https://doi.org/10.1039/C4EE00942H.
34. Ganesan P., Fu K., Gao P. **(2015)** A simple spiro-type hole transporting material for efficient perovskite solar cells. *Energy Environ. Sci.*, 8, 1986–1991. https://doi.org/10.1039/C4EE03773A.
35. Sun ZZ., Xu YL., Zhu R., Liu HY. **(2018)** How to stabilize the HOMO levels and improve the charge transport properties of hole-transporting materials. *Org. Electron.*, 63, 86–92. https://doi.org/10.1016/j.orgel.2018.09.013.
36. Aboulouard A., Arif A., Can M, El idrissi M. **(2024)** Engineering quinoxaline-based non-fullerene acceptors for high-performance organic solar cells: A DFT and TD-DFT study. *Mater. Chem. Phys.,* 310, 127993. https://doi.org/10.1016/j.matchemphys.2024.127993.
37. Wang T., Xie Y., Dou Y. **(2018)** Design and investigation of carbazole-based hole transport materials for perovskite solar cells. *Synthetic Metals.*, 235, 9–18. https://doi.org/10.1016/j.synthmet.2017.11.013.
38. Shi GZ., Wang YK., Yuan ZC. **(2016)** Dopant-free spiro-triphenylamine/fluorene hole-transporting material for perovskite solar cells. *Adv. Funct. Mater.*, 26(9), 1375–1381. https://doi.org/10.1002/adfm.201504245.
39. Fantacci S., De Angelis F., Nazeeruddin MK., Grätzel M. **(2011)** Electronic and optical properties of the Spiro-MeOTAD hole conductor in its neutral and oxidized forms: A DFT/TDDFT investigation. *J. Phys. Chem. C.*, 115(46), 23126–23133. https://doi.org/10.1021/jp207968b.
40. Sun ZZ., Xu YL., Zhu R., Liu HY. **(2018)** Probing the effects of molecular symmetry on the HOMO levels and charge transport properties of hole-transporting materials. *Org. Electron.*, 63, 86–92. https://doi.org/10.1016/j.orgel.2018.09.013.
41. Aboulouard A., Arif A., Kerraj S., El idrissi M. **(2025)** Novel quinoxaline derivatives as donor materials for bulk heterojunction organic solar cells: DFT and TD-DFT insights. *Synthetic Metals.*, 305, 116851. https://doi.org/10.1016/j.synthmet.2024.116851.
42. Nikzad-Langerodi R., Sarvari N., Razi N., Behjati S. **(2017)** Theoretical design of spiro-based hole transporting materials for perovskite solar cells. *Org. Electron.*, 50, 191–199. https://doi.org/10.1016/j.orgel.2017.07.035.
43. Ganesan P., Fu K., Gao P. **(2015)** A simple spiro-type hole transporting material for efficient perovskite solar cells. *Energy Environ. Sci.*, 8, 1986–1991. https://doi.org/10.1039/C4EE03773A.
44. Wang T., Xie Y., Dou Y. **(2018)** Theoretical design and investigation of carbazole-based hole transport materials for perovskite solar cells. *Synth. Met.*, 235, 9–18. https://doi.org/10.1016/j.synthmet.2017.11.013.
45. Sun ZZ., Xu YL., Zhu R., Liu HY. **(2018)** How to stabilize the HOMO levels and improve the charge transport properties of hole-transporting materials?. *Org. Electron.*, 63, 86–92. https://doi.org/10.1016/j.orgel.2018.09.013.
46. Aboulouard A, Arif A, Kerraj S, El idrissi M. **(2025)** Engineering quinoxaline-based non-fullerene acceptors for organic solar cells: A combined DFT and TD-DFT study. *Synth. Met.*, 305, 116851. https://doi.org/10.1016/j.synthmet.2024.116851.
47. Diany R., Kerraj S,. Atouailaa MK,. Arif A,. Aboulouard A,. Boulghalat M,. Tounsi A,. Salah M,. El idrissi M. **(2025)** Enhancing the electronic and optical performance of dye-sensitized solar cells with alizarin-based dyes: DFT/TDDFT investigations. *Curr. Chem. Lett.,* 14(3), 597-612. https://doi.org/10.5267/j.ccl.2025.2.006.
48. Diany R., Kerraj S., Aboulouard A., Syed A., Zeroual A., Bahkali A.H., Salah M., El idrissi M. **(2024)** Enhancing dye sensitized solar cells performance through quinoxaline based organic dye sensitizers. *J. Comput. Electron.,* 1-14. https://doi.org/10.1007/s10825-024-02211-3
49. Guerra CF., Snijders JG., te Velde G., Baerends EJ. **(1998)** Towards an order-N DFT method. *Theor. Chem. Acc.*, 99(6), 391–403. https://doi.org/10.1007/s002140050353

© 2025 by the authors; licensee Growing Science, Canada. This is an open access article distributed under the terms and conditions of the Creative Commons Attribution (CC-BY) license (http://creativecommons.org/licenses/by/4.0/).